



Low-energy electron impact dissociative recombination and vibrational transitions of N_2^+

A. Abdoulanziz, C. Argentin, V. Laporta, K. Chakrabarti, Arnaud Bultel, J. Tennyson, I. Schneider, J. Zs. Mezei

► To cite this version:

A. Abdoulanziz, C. Argentin, V. Laporta, K. Chakrabarti, Arnaud Bultel, et al.. Low-energy electron impact dissociative recombination and vibrational transitions of N_2^+ . Journal of Applied Physics, 2021, 129 (5), pp.053303. 10.1063/5.0038609 . hal-03140994

HAL Id: hal-03140994

<https://hal.science/hal-03140994>

Submitted on 9 Jan 2024

HAL is a multi-disciplinary open access archive for the deposit and dissemination of scientific research documents, whether they are published or not. The documents may come from teaching and research institutions in France or abroad, or from public or private research centers.

L'archive ouverte pluridisciplinaire **HAL**, est destinée au dépôt et à la diffusion de documents scientifiques de niveau recherche, publiés ou non, émanant des établissements d'enseignement et de recherche français ou étrangers, des laboratoires publics ou privés.

Low-energy electron impact dissociative recombination and vibrational transitions of N_2^+

A. Abdoulanziz¹, C. Argentin^{1,2}, V. Laporta³, K. Chakrabarti⁴,
A. Bultel², J. Tennyson^{5,1}, I. F. Schneider^{1,6}, and J. Zs Mezei^{7,1*}

¹LOMC CNRS-UMR6294, Université le Havre Normandie, F-76058 Le Havre, France

²CORIA-UMR6614 CNRS-Université de Rouen Normandie, 76800 Saint-Etienne du Rouvray, France

³Istituto per la Scienza e Tecnologia dei Plasmi, CNR, 70126 Bari, Italy

⁴Dept. of Mathematics, Scottish Church College, 700006 Kolkata, India

⁵Dept. of Physics and Astronomy, University College London, WC1E 6BT London, UK

⁶LAC CNRS-FRE2038, Université Paris-Saclay, F-91405 Orsay, France and

⁷Institute for Nuclear Research (ATOMKI), H-4001 Debrecen, Hungary

(Dated: February 25, 2022)

Cross sections and thermal rate coefficients are computed for electron-impact dissociative recombination and vibrational excitation/de-excitation of the N_2^+ molecular ion in its lowest six vibrational levels, for collision energies/temperatures up to 2.3 eV/5000 K.

I. INTRODUCTION

The nitrogen molecule N_2 is one of the most widely studied species so far in plasma physics. Being very stable at low temperature, it is very abundant in the Earth atmosphere, and is notably present in other planetary atmospheres - Titan 98.4 % [1], Triton [2] Pluto [3], Venus 3.5 % and Mars 1.9 % [1]. For other trans-Neptunian objects than Pluto, this molecule is also one of the main component of the ices - spectroscopically observed at their surfaces - and may produce a very thin atmosphere when the temperature increases under solar irradiation [4]. Under the influence of an electric field, high altitude planetary atmosphere can be crossed by giant discharges of a few milliseconds duration called sprites, whose spectroscopic signature is mainly due to spontaneous emission from N_2 excited electronic states [5]. The application of N_2 as seeding gas in magnetically confined fusion plasmas (ITER and JET equipments) will help in the reduction of power loads on the tungsten divertor region. Nitrogen may be preferable as an extrinsic radiator to noble gases (neon) as it mostly affects the divertor radiation without significantly increasing core radiation [6, 7].

All this facts justify the various studies of the role of the N_2 molecule in the cold plasmas, from the state-to-state description of its electron impact induced reactivity [8–10] to the detailed modeling of its contribution to the plasma kinetics [11–14].

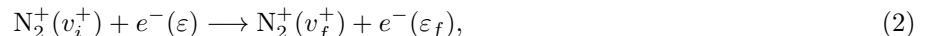
Consequently, the N_2^+ cation is also of huge interest. Due to the solar irradiation, the production of N_2^+ on excited vibrational states plays a significant role in the characteristics of the Earth's thermosphere [15]. It is also the main molecular cation in the atmosphere of Titan [16] and Triton [17]. On the other hand, during the atmospheric entry of a spacecraft in Earth's and Titan's atmospheres, the hypersonic compression of the gases leads to the formation of a plasma departing from local thermodynamic equilibrium [18]. The ionic composition, including N_2^+ , plays a key role in the radiation emitted by the plasma in the near UV spectral region [19]. In many plasma-assisted industrial processes elaborated so far, the plasma reactivity is greatly enhanced by the presence of N_2^+ . This is, for instance, the case in the ammonia synthesis in plasmas/liquid processes [20]. N_2^+ is also very effective in the antibacterial treatment of polyurethane surfaces [21]. Moreover, N_2^+ - like N_2 - is a key ingredient in the steel nitriding, resulting in the improving of its frictional wear resistance, surface hardness and corrosion resistance [22]. Furthermore, N_2^+ also plays a major role in the dermatological treatments based on the nitrogen radio-frequency discharges [23].

The characteristics of the nitrogen-containing plasmas cannot be fully understood without a deep knowledge of the reactivity of N_2^+ , in particular by collisions with electrons.

Dissociative Recombination (DR) is the major molecular cation destruction reaction, that takes place when an electron collides with the N_2^+ molecular cation, leading to neutral atomic fragments:



Here ε is kinetic energy of the incident electron and v_i^+ the initial vibrational quantum number of the target. Alongside DR, other competitive processes can occur:



*mezei.zsolt@atomki.hu

i.e. elastic (EC) ($v_f^+ = v_i^+$), inelastic (IC) ($v_f^+ > v_i^+$) and super-elastic (SEC) collisions ($v_f^+ < v_i^+$), v_f^+ standing for the final vibrational quantum number of the target ion. These processes are also known as Elastic Scattering (ES), Vibrational Excitation (VE) and Vibrational deExcitation (VdE) respectively.

The elementary non-thermal electron driven processes, in particular dissociative recombination, has been studied experimentally using plasmas with laser induced photo-fluorescence techniques [24], shock tubes [25], discharge afterglow experiments [26, 27] and microwave techniques [28]. The most detailed collisional data can be obtained in merged beam [29] and/or storage ring experiments [30].

Two different sets of theoretical calculations have been performed [31–34] on the DR of N_2^+ . They involved different underlying quantum chemistry but rather similar nuclear dynamics calculations; both these studies focused on the ground and the lowest three vibrational levels of the N_2^+ target.

While both results show good agreement with experiment for the ground vibrational level, the rates for the higher vibrational levels calculated in [31], contrary to those of [32–34], indicate less strong vibrational dependence on temperature, in agreement with the experimental results.

Our aim with this paper is to extend as far as possible the calculations started in [31]. This extension refers to:

- i) the kinetic energy of the incoming electron: up to 2.3 eV *vs* 1 eV previously.
- ii) the elementary processes explored: besides the DR studied in the past, the VE and VdE cross sections and rate coefficients are computed.
- iii) the vibrational levels considered in the vibrational transitions: up to the fifth excited level of the target *vs* the third previously, and the lowest ten vibrational levels as final ones.

The rotational effects have been neglected, since they are important only at very low collision energies.

All these extensions make our results relevant for the atmospheric and cold plasma environments, at electron temperatures where the rotational effects can be neglected.

The paper is organized as follows: After a brief description of the theoretical approach (section II), we present in more details the molecular data used in the calculations (section III) followed by the presentation of the results (section IV). The paper is ended by conclusions.

II. THEORETICAL APPROACH

The efficiency of our method of modeling the electron/diatomic cation collisions, based on the Multichannel Quantum Defect Theory (MQDT) has been proved in many previous studies on different species, including H_2^+ and its isotopologues [35–37], ArH^+ [38], CH^+ [39], SH^+ [40], etc. The general ideas of our approach were already presented in detail in our previous study of the N_2^+ dissociative recombination [31] and, therefore, here we restrict ourselves to its major steps.

The reactive processes (1) and (2) involve *ionization* channels - describing the scattering of an electron on the target cation - and *dissociation* channels - accounting for atom-atom scattering. The mixing of these channels results in quantum interference of the *direct* mechanism - in which the capture takes place into a doubly excited dissociative state of the neutral system - and the *indirect* one - in which the capture occurs via a Rydberg bound state of the molecule belonging to a *closed* channel, this state being predissociated by the dissociative one. In both mechanisms the autoionization - based on the existence of *open* ionization channels - is in competition with the predissociation, and can lead to the excitation or to the de-excitation of the cation.

One starts with the building of the *interaction matrix* \mathbf{V} that drives the collision, whose elements quantify the couplings between the different channels - ionization and/or dissociation ones.

More specifically, each of the ionization channels, built on the N_2^+ ion in one of its three lowest electronic states - $X^2\Sigma_g^+$, $A^2\Pi_u$ or $B^2\Sigma_u^+$, see Fig. 1 - in a particular vibrational level, interacts not only with all the dissociation exit channels (Rydberg-valence interaction), but also with the other ionization channels (Rydberg-Rydberg interactions) - Fig. 2. Depending on the total energy of the system these ionization channels can be *open* - either as entrance channels, describing the incident electron colliding the ion in its ground electronic state, or exit channels, describing the auto-ionization, i.e. elastic scattering, vibrational excitation and de-excitation - or *closed* - describing the resonant temporary captures into Rydberg states.

Once the \mathbf{V} -matrix is elaborated, we build the short-range reaction matrix \mathbf{K} of the collision, as a second order perturbative solution of the Lippmann-Schwinger equation. The diagonalized version of the \mathbf{K} -matrix (in the eigenchannel representation) whose eigenvalues are expressed in terms of long range phase-shifts of the eigenfunctions, together with the vibronic couplings between the ionization channels, serve for the building of the frame transformation matrices.

Applying a Cayley transformation on these latter matrices we can set up the generalized scattering matrix \mathbf{X} . The Seaton's method of 'eliminating' the closed channels [41] is then employed, resulting in the physical scattering matrix \mathbf{S} :

$$\mathbf{S} = \mathbf{X}_{oo} - \mathbf{X}_{oc} \frac{1}{\mathbf{X}_{cc} - \exp(-i2\pi\nu)} \mathbf{X}_{co}, \quad (3)$$

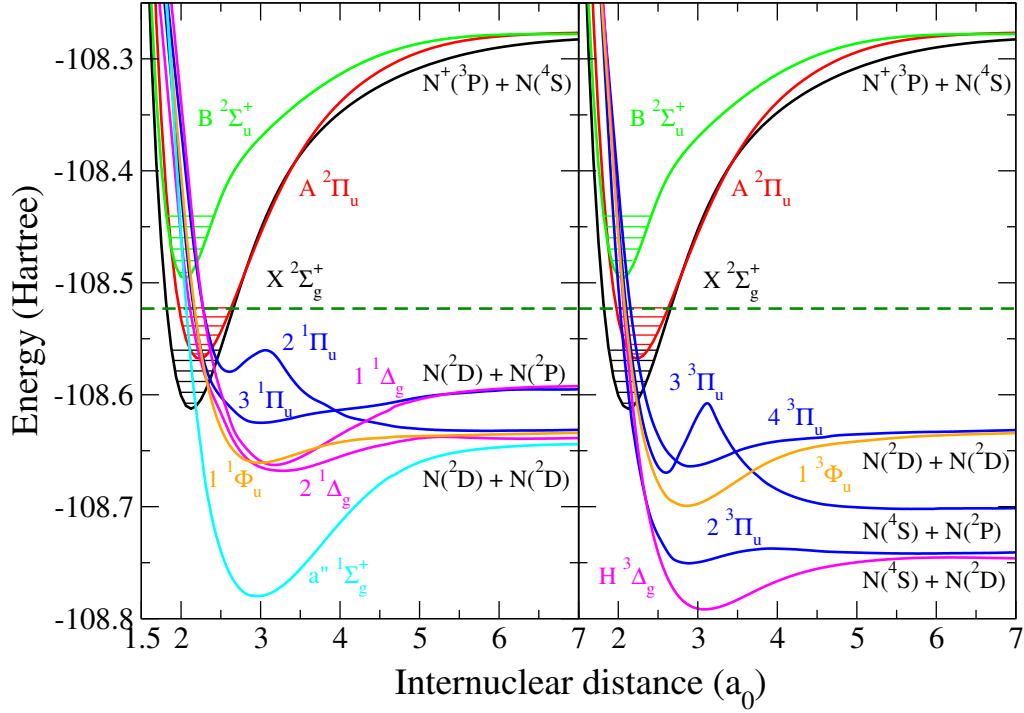


FIG. 1: Potential energy curves (PEC) relevant for the DR of N_2^+ [31]. Target cation N_2^+ : ground electronic state ($X^2\Sigma_g^+$) black, first excited state ($A^2\Pi_u$) red, second excited state $B^2\Sigma_u^+$ green. Neutral system N_2 : Left panel, singlet states of different symmetries - blue for $^1\Pi_u$, magenta for $^1\Delta_g$, cyan for $a'^1\Sigma_g^+$ and orange for $^1\Phi_u$. Right panel, triplet states of different symmetries - blue for $^3\Pi_u$, magenta for $H^3\Delta_g$ and orange for $^3\Phi_u$. The lowest five vibrational levels of each electronic state of the ion and the dissociative asymptotic limits for all states are shown. The green dashed line gives the upper limit of the total energy of the system, above which our results are still reasonably correct (see text).

relying on the block-matrices involving open (\mathbf{X}_{oo}), open and closed (\mathbf{X}_{oc} and \mathbf{X}_{co}) and closed (\mathbf{X}_{cc}) channels. The diagonal matrix $\boldsymbol{\nu}$ in the denominator of equation (3) contains the effective quantum numbers corresponding to the vibrational thresholds of the closed ionisation channels at given total energy of the system.

Finally, the cross section for the dissociative recombination and for the vibrational transitions - vibrational excitation/ de-excitation and elastic scattering write respectively as:

$$\sigma_{diss \leftarrow v_i^+} = \frac{\pi}{4\varepsilon} \rho^{sym} \sum_{l,j} \left| S_{d_j,lv_i^+}^\Lambda \right|^2$$

and

$$\sigma_{v_f^+ \leftarrow v_i^+} = \frac{\pi}{4\varepsilon} \rho^{sym} \sum_{l,l'} \left| S_{l'v_f^+,lv_i^+}^\Lambda - \delta_{l,l'} \delta_{v_i^+,v_f^+} \right|^2. \quad (4)$$

where d_j stands for a given dissociative state and ρ^{sym} the ratio between the state-multiplicities of the neutral and the target ion.

III. MOLECULAR DATA

The nuclear dynamics in low-energy electron/molecular cation collisions crucially depends on the molecular structure of the target and of the formed neutral - often superexcited - complex. The relevant molecular data sets consist in the potential energy curves (PECs) of the target cation - for the ground and for the excited electronic states - the PECs of the doubly excited bound or dissociative molecular states of the neutral, the quantum defect-functions characterizing the bound mono-excited Rydbers series of the neutral, and the coupling functions between the several - ionization and dissociation - continua.

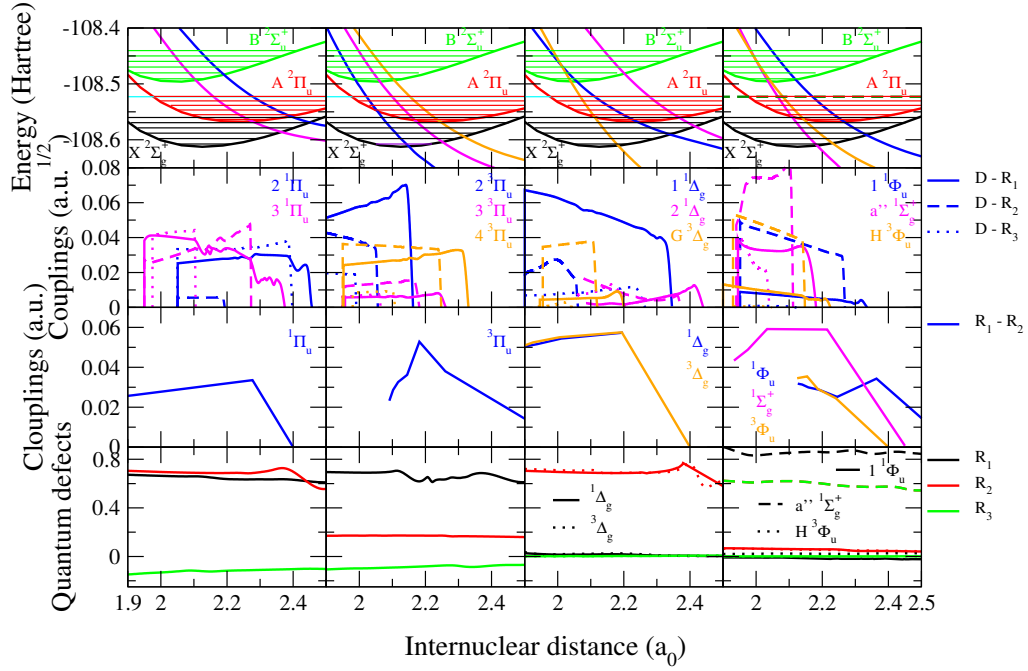


FIG. 2: Molecular data sets for the modeling of reactive collisions between electrons and N_2^+ [31]. 1st row: PECs of the relevant states of the ion and of the neutral for all relevant symmetries. 2nd row: Rydberg-valence electronic couplings. 3rd row: Rydberg-Rydberg electronic couplings. 4th row: Quantum defects characterizing the Rydberg series of states.

One of the few quantum chemistry methods capable of producing the highly-excited molecular states at the required accuracy is based on the R-Matrix Theory [42]. Bound and resonant adiabatic potential energy curves of the valence and Rydberg states of N_2 having singlet and triplet symmetries were obtained by Little and Tennyson [43, 44] using R-matrix calculations on fine grid of internuclear separations. The diabatic curves, couplings and quantum defects relevant for the dissociative recombination of N_2^+ were presented in [31]. The electronic states of the target were calculated using the standard quantum chemistry program suite Molpro [45]. Figure 1 shows the PECs of the dissociative molecular states of N_2 , as well as those of the relevant states of N_2^+ , involved in our previous [31] and present calculations.

The same PECs are displayed by symmetries on the first row of Figure 2, which contains the whole ensemble of molecular data relevant for the modeling of the internuclear dynamics. Whereas its first row illustrates how favorable the crossings are between the PECs of the dissociative states with those of the target ones - i.e. the Franck-Condon effect - the driving interactions of the dynamics - the Rydberg-valence couplings - are shown in the second row. The third row gives the Rydberg-Rydberg couplings: In the present calculation, only the couplings among the series correlating to the ground (X) and first excited (A) state of the ion have been considered. And finally the last row of the figure displays the quantum defects characterizing the Rydberg series built, each of them, on one of the three cores X , A and B .

IV. RESULTS AND DISCUSSIONS

Based on the molecular data already presented in fig. 2, we have performed the nuclear dynamics calculations using the MQDT approach presented in Section II. The DR, VE and VdE cross sections have been calculated considering the N_2^+ target in one of its lowest six vibrational states, and focusing on the vibrational transitions to the lowest ten vibrational levels, when energetically accessible. Table I shows the energies of these latter levels relative to $v_i^+ = 0$ of the target.

The calculations have been performed by taking into account both the *direct* and the *indirect* mechanisms, the reaction matrix being evaluated in the second order, and all their vibrational levels - 81, 66 and 50 respectively, associated to *open* or *closed* ionization channels, according to the total energy of the system - have been fully accounted.

The cross sections have been calculated for all the relevant symmetries listed in figs. 1 and 2, for collision energies of the incident electron ranging between 10^{-5} and 2.3 eV, with an energy step of 0.01 meV. These cross sections have been summed up to obtain the global cross sections.

TABLE I: The energies of the vibrational levels of the N_2^+ molecular cation - relative to the ground one - involved either as initial or as final levels in the present calculations.

v^+	0	1	2	3	4	5	6	7	8	9
E_{v^+} (eV)	0.0	0.266	0.528	0.786	1.040	1.290	1.536	1.777	2.014	2.248

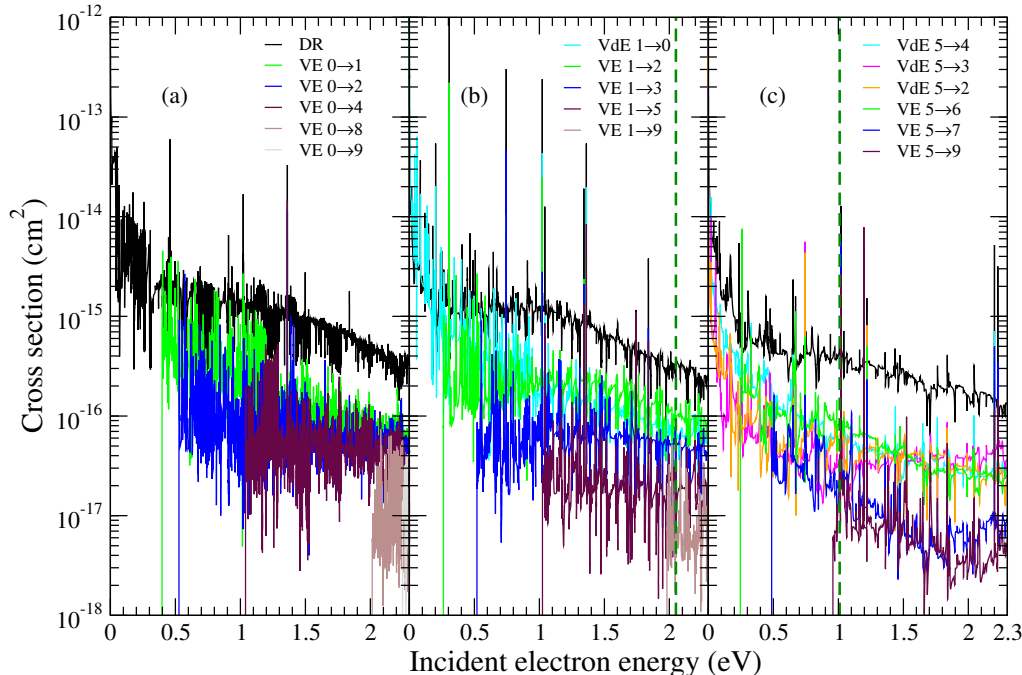


FIG. 3: Global DR, VE and VdE cross sections of the N_2^+ $v_i^+ = 0$ (a), $v_i^+ = 1$ (b) and $v_i^+ = 5$ (c) as a function of the collision energy. For vibrational transitions (VE and VdE) we label the processes as transitions from the initial to the final vibrational levels of the target. The vertical dashed dark-green line gives the precision limit of the calculations (for details see text).

The global DR, VE and VdE cross sections for target cations having initial vibrational levels $v_i^+ = 0, 1$ and 5 are shown in figure 3 (a), (b) and (c) panels respectively. The vertical dark-green dashed lines in the mid and upper panels of figure 3 mark the energy below which the calculations are the most accurate. Above these thresholds the calculations neglect the role of the higher lying dissociative states of the neutral.

Nevertheless, the data displayed continue to be reasonably correct above these thresholds because these dissociative states penetrate into the ionization continuum well above these thresholds, forming favourable/non-vanishing Franck-Condon overlaps with the target electronic states at even higher collision energies. This Franck-Condon overlap is proportional with the first order term of the direct cross section. In addition the couplings of these dissociative states with the Rydberg series are generally weaker, leading to less important cross sections in second order.

The *direct* mechanism is responsible for the background $1/E$ behaviour of the cross sections, while the *indirect* one through the temporary capture into the Rydberg states produces all the resonance structures dominating the cross sections.

Among all the processes studied here dissociative recombination (black curves in fig. 3) predominates. The global DR cross section increases as we change the initial vibrational state of the target by unity and starts to decrease as we arrive at $v_i^+ = 5$. While the vibrational de-excitation (cyan curves for initial vibrational levels higher than 0) are in competition with the DR cross section, at higher collision energies their overall cross section values are at least with a factor of 5 smaller than those of the DR. The vibrational excitations (green, blue, violet, maroon, etc. curves) show threshold effects at the collision energies where they become open. Moreover, one can see that for a given initial vibrational level v_i^+ the $|\Delta v^+| = 1$ vibrational transitions are the most probable ones, decreasing monotonically with $|\Delta v^+|$ for the transitions between more distant levels.

Figure 4 shows the thermal rate coefficients of all processes for the six lowest initial vibrational levels of N_2^+ . The green dashed line gives the precision limits of our calculation expressed now in electron temperatures.

The DR (solid black line in figure 4) and VdE (symbols and thick coloured lines) rate coefficients decrease mono-

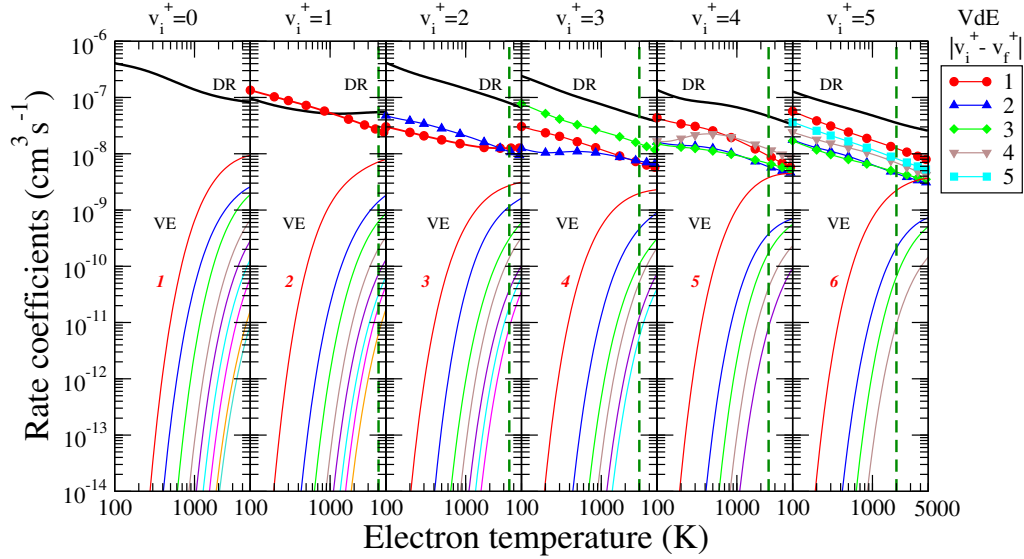


FIG. 4: Maxwell rate coefficients for all the relevant electron-induced processes on N_2^+ initially on $v_i^+ = 0 - 5$ vibrational levels : Dissociative recombination (black line), vibrational excitation (thin coloured lines) and vibrational de-excitation (symbols and thick coloured lines). For the vibrational excitations all the transitions are shown up to $v_f^+ = 9$ with the lowest transition being labeled on each figure. The excitation and the de-excitation up to the final vibrational quantum numbers are given. The green dashed line gives the precision limit of our calculation given in temperatures (for details see text).

TABLE II: List of the fitting parameters used in formula (5), temperature regions and root mean squares for the DR rate coefficients of N_2^+ ($v_i^+ = 0 - 5$).

v_i^+	Temperature range K	A ($cm^3 s^{-1} K^{-\alpha}$)	α	B (K)	RMS
DR 0	$100 \leq T \leq 700$	1.56020×10^{-5}	-0.679449	53.0333	0.0051
	$700 < T \leq 5000$	2.27099×10^{-7}	-0.129049	-388.399	0.0040
1	$100 \leq T \leq 900$	1.11178×10^{-7}	-0.120373	-41.6843	0.0049
	$900 < T \leq 5000$	2.60704×10^{-8}	0.086645	-85.4307	0.0055
2	$100 \leq T \leq 1000$	1.54430×10^{-6}	-0.345836	-28.1712	0.0053
	$1000 < T \leq 5000$	7.09592×10^{-6}	-0.544674	145.630	0.0030
3	$100 \leq T \leq 5000$	1.53033×10^{-6}	-0.438705	-19.1368	0.0088
4	$100 \leq T \leq 460$	5.25573×10^{-8}	0.042384	-76.5345	0.0032
	$460 < T \leq 5000$	3.42600×10^{-6}	-0.539469	208.028	0.0031
5	$100 \leq T \leq 5000$	7.20627×10^{-7}	-0.394354	-7.90548	0.0106

tonically with the temperature, while the VE (thin coloured lines) ones increase, partly because of the threshold behaviour of their corresponding cross sections. The largest rate coefficients we obtained are those for the DR. With the exception of the $v_i^+ = 1$ case the VdE rate coefficients are smaller than those for the DR. At $v_i^+ = 1$, the DR is in competition with VdE but, for $v_i^+ > 1$ DR exceeds VdE with a factor of 2 – 5. We can see from figure 4 that the VE process is relatively important at high electron temperatures only. Moreover, higher we go with the initial vibrational quantum number of the target cation, more probable VE becomes.

And finally, in order to allow the versatile implementation of the rate coefficients in kinetics modelling codes, we have fitted them with Arrhenius-type formulas. The calculated rate coefficients for the dissociative recombination of electrons with N_2^+ on each of its lowest 6 vibrational levels ($v_i^+ = 0, 1, \dots, 5$) have been interpolated under the mathematical form:

$$k^{fitt}(T) = A T^\alpha \exp \left[-\frac{B}{T} \right] \quad (5)$$

over the electron temperature range $100 \text{ K} \leq T_e \leq 5000 \text{ K}$ and/or for rate coefficients larger than $10^{-14} \text{ cm}^3 \text{ s}^{-1}$, as displayed in fig. 4. The A , α and B fitting parameters used in equation (5) together with the temperature regions are listed in table II for DR, and in table III for VE and VdE processes. The efficiency of the fitting are characterised with the Root Mean Squares, and we were able to reproduce the MQDT rate coefficients with a precision higher than 97%.

TABLE III: List of the fitting parameters used in formula (5), temperature regions and root mean squares for the VE and VdE rate coefficients of N_2^+ ($v_i^+ = 0 - 5$ and $v_f^+ = 9$). The lines having bold v_f^+ values belong to VdE.

v_i^+	v_f^+	Temperature range (K)	A ($cm^3 s^{-1} K^{-\alpha}$)	α	B (K)	RMS	v_i^+	v_f^+	Temperature range (K)	A ($cm^3 s^{-1} K^{-\alpha}$)	α	B (K)	RMS
0	1	270 ≤ T ≤ 5000	3.35476×10^{-6}	-0.584062	4525.43	0.0073	3	0	100 ≤ T ≤ 700	3.69265×10^{-7}	-0.399263	-29.4462	0.0087
	2	400 ≤ T ≤ 1000	9.13678×10^{-7}	-0.553899	6100.88	0.0021			700 < T ≤ 5000	1.88955×10^{-6}	-0.594995	205.425	0.0045
		1000 < T ≤ 5000	3.04596×10^{-7}	-0.420925	5907.02	0.0028	4		100 ≤ T ≤ 560	3.67969×10^{-7}	-0.546948	2807.96	0.0290
	3	600 ≤ T ≤ 1500	9.67070×10^{-7}	-0.509170	3228.55	0.0062			560 < T ≤ 5000	1.29198×10^{-7}	-0.410534	2682.71	0.0112
		1500 < T ≤ 5000	4.98432×10^{-6}	-0.699380	9626.89	0.0040	5		440 ≤ T ≤ 1300	4.82997×10^{-7}	-0.335457	5887.42	0.0106
	4	850 ≤ T ≤ 2000	9.30628×10^{-8}	-0.292379	11989.3	0.0054			1300 < T ≤ 5000	8.49983×10^{-9}	-0.137448	5427.34	0.0084
		2000 < T ≤ 5000	8.81469×10^{-7}	-0.546342	12651.0	0.0033	6		650 ≤ T ≤ 1700	1.54145×10^{-7}	-0.532191	9039.15	0.0032
	5	1000 ≤ T ≤ 5000	8.92493×10^{-7}	-0.596125	14871.8	0.0066			1300 < T ≤ 5000	9.06525×10^{-10}	0.052019	7617.98	0.0111
	6	1200 ≤ T ≤ 2500	1.44702×10^{-6}	-0.667566	17980.5	0.0022	7		850 ≤ T ≤ 2000	2.49601×10^{-8}	-0.300658	11333.8	0.0091
		2500 < T ≤ 5000	5.49126×10^{-6}	-0.815886	18422.2	0.0009			2000 < T ≤ 5000	4.15424×10^{-9}	-0.093853	10888.7	0.0003
	7	1500 ≤ T ≤ 5000	1.65552×10^{-6}	-0.696318	21345.0	0.0190	8		1100 ≤ T ≤ 5000	2.27558×10^{-9}	-0.079760	13723.8	0.0189
	8	1800 ≤ T ≤ 5000	9.86709×10^{-8}	-0.470871	23504.3	0.0071	9		1300 ≤ T ≤ 5000	3.06856×10^{-7}	-0.645208	17278.8	0.0034
	9	2000 ≤ T ≤ 5000	1.34002×10^{-6}	-0.780327	26309.7	0.0025	4	3	100 ≤ T ≤ 400	6.37863×10^{-8}	-0.145968	-28.4720	0.0082
1	0	100 ≤ T ≤ 5000	1.45341×10^{-6}	-0.478820	19.3876	0.0195			400 < T ≤ 5000	6.36181×10^{-6}	-0.825697	192.216	0.0072
	2	190 ≤ T ≤ 900	3.82842×10^{-6}	-0.706740	3146.96	0.0154	2		100 ≤ T ≤ 900	6.55402×10^{-8}	-0.262797	23.6274	0.0227
		900 < T ≤ 5000	1.45126×10^{-8}	-0.015912	2326.31	0.0076			900 < T ≤ 5000	1.05821×10^{-7}	-0.378427	-214.371	0.0140
	3	420 ≤ T ≤ 900	1.79064×10^{-7}	-0.420497	6137.15	0.0011	1		100 ≤ T ≤ 440	2.32972×10^{-8}	-0.116666	-8.97262	0.0057
		900 < T ≤ 5000	1.14329×10^{-8}	-0.080877	5736.89	0.0040			440 ≤ T ≤ 5000	2.27097×10^{-7}	-0.444141	124.096	0.0044
	4	600 ≤ T ≤ 1500	5.53686×10^{-8}	-0.277018	8726.55	0.0040	0		100 ≤ T ≤ 400	2.12911×10^{-9}	0.389295	-22.4417	0.0183
		1500 < T ≤ 5000	4.12085×10^{-7}	-0.506359	9262.99	0.0065			400 < T ≤ 5000	2.10016×10^{-6}	-0.645580	264.431	0.0066
	5	850 ≤ T ≤ 5000	1.38279×10^{-7}	-0.426255	12008.4	0.0031	5		190 ≤ T ≤ 900	7.69858×10^{-7}	-0.525187	2964.92	0.0217
	6	1100 ≤ T ≤ 2500	9.87396×10^{-7}	-0.707100	14813.1	0.0035			900 < T ≤ 5000	2.43298×10^{-6}	-0.666480	3146.71	0.0028
		2500 < T ≤ 5000	3.02402×10^{-8}	-0.318434	13684.3	0.0017	6		400 ≤ T ≤ 1200	4.49741×10^{-6}	-0.896475	5955.41	0.0017
	7	1300 ≤ T ≤ 5000	3.25083×10^{-8}	-0.336661	16732.0	0.0157			1200 < T ≤ 5000	8.84487×10^{-7}	-0.708372	5563.92	0.0076
	8	1500 ≤ T ≤ 5000	1.39545×10^{-7}	-0.467278	20348.3	0.0062	7		580 ≤ T ≤ 1500	1.17991×10^{-5}	-0.974002	8780.06	0.0036
	9	1800 ≤ T ≤ 5000	3.50537×10^{-8}	-0.362041	22692.0	0.0027			1500 < T ≤ 5000	7.34677×10^{-7}	-0.655786	8053.50	0.0084
2	1	100 ≤ T ≤ 1500	1.04603×10^{-7}	-0.287973	-9.07849	0.0073	8		800 ≤ T ≤ 2000	4.10791×10^{-6}	-0.886512	11434.1	0.0015
		1500 < T ≤ 5000	4.35037×10^{-9}	0.116715	-377.074	0.0027			2000 < T ≤ 5000	3.73224×10^{-7}	-0.615368	10737.3	0.0026
	0	100 ≤ T ≤ 5000	6.63440×10^{-7}	-0.498417	38.4238	0.0193	9		1000 ≤ T ≤ 2500	1.13754×10^{-7}	-0.519202	13677.4	0.0126
	3	200 ≤ T ≤ 700	1.79199×10^{-7}	-0.415799	2977.42	0.0005			2500 < T ≤ 5000	1.25100×10^{-8}	-0.269595	13039.9	0.0002
		700 < T ≤ 5000	7.47837×10^{-8}	-0.306566	2843.67	0.0089	5	4	100 ≤ T ≤ 5000	4.50970×10^{-7}	-0.474388	-11.0566	0.0125
	4	400 ≤ T ≤ 1300	4.27598×10^{-6}	-0.800392	6144.90	0.0036			100 ≤ T ≤ 500	5.83098×10^{-8}	-0.304037	-19.8859	0.0073
		1300 < T ≤ 5000	4.37539×10^{-8}	-0.268995	5056.36	0.0148			500 < T ≤ 5000	1.31781×10^{-7}	-0.447966	-55.6242	0.0132
	5	600 ≤ T ≤ 1500	7.02948×10^{-8}	-0.367691	8687.59	0.0076	2		100 ≤ T ≤ 5000	6.21686×10^{-8}	-0.340696	-27.4858	0.0101
		1500 < T ≤ 5000	8.34212×10^{-9}	-0.117668	8217.86	0.0022	1		100 ≤ T ≤ 900	8.49509×10^{-8}	-0.310555	-17.4355	0.0022
	6	850 ≤ T ≤ 5000	9.67864×10^{-8}	-0.401678	11429.0	0.0164			900 < T ≤ 5000	1.08934×10^{-6}	-0.653000	198.309	0.0031
	7	1000 ≤ T ≤ 2500	9.38561×10^{-7}	-0.733592	14527.8	0.0013	0		100 ≤ T ≤ 5000	3.73256×10^{-7}	-0.501538	2.80363	0.0122
		2500 < T ≤ 5000	1.75259×10^{-7}	-0.547538	13960.8	0.0012	6		190 ≤ T ≤ 5000	1.47602×10^{-7}	-0.367489	2789.39	0.0150
	8	1300 ≤ T ≤ 5000	1.13024×10^{-6}	-0.737221	17518.6	0.0117	7		400 ≤ T ≤ 1200	3.15877×10^{-8}	-0.292229	5543.78	0.0036
	9	1500 ≤ T ≤ 5000	1.46292×10^{-7}	-0.513870	19732.3	0.0137			1200 < T ≤ 5000	1.10525×10^{-6}	-0.712115	6289.63	0.0090
3	2	100 ≤ T ≤ 5000	3.60161×10^{-7}	-0.490909	23.3038	0.0108	8		600 ≤ T ≤ 5000	4.10724×10^{-7}	-0.585006	8593.14	0.0153
	1	100 ≤ T ≤ 700	2.52673×10^{-9}	0.215750	-58.7472	0.0174	9		850 ≤ T ≤ 2000	7.61666×10^{-7}	-0.744946	11307.6	0.0038
		700 ≤ T ≤ 5000	7.86265×10^{-8}	-0.292543	41.8077	0.0060			2000 < T ≤ 5000	7.87895×10^{-8}	-0.489941	10618.0	0.0036

V. CONCLUSIONS

The present work extends considerably our previous study of the dissociative recombination of N_2^+ with electrons [31]. Making use of the molecular data set calculated in Refs. [31, 43, 44] and of our step-wise MQDT method, we have performed calculations for the lowest 6 vibrational levels of the target cation in collision with electrons having kinetic energy up to 2.3 eV and, in the case of thermal equilibrium, electronic temperature up to 5000 K. We have provided cross sections and rate coefficients for dissociative recombination, vibrational excitation and de-excitation of N_2^+ molecular cation, important for the detailed kinetic modelling of cold astrophysical, atmospheric and laboratory plasmas. The calculated cross sections and rate coefficients are available on request.

Acknowledgments

The authors acknowledge support from Fédération de Recherche Fusion par Confinement Magnétique (CNRS and CEA), La Région Normandie, FEDER and LabEx EMC3 via the projects PTOLEMEE, Bioengine, EMoPlaF, COMUE Normandie Université, the Institute for Energy, Propulsion and Environment (FR-IEPE), the European Union via COST (European Cooperation in Science and Technology) action MD-GAS (CA18212), and ERASMUS-plus conventions between Université Le Havre Normandie and University College London. This work has received funding from the Euratom research and training programme 2014-2018 and 2019-2020 under grant agreement No. 633053. The views and opinions expressed herein do not necessarily reflect those of the European Commission. We

are indebted to Agence Nationale de la Recherche (ANR) via the project MONA, Centre National de la Recherche Scientifique via the GdR TheMS and the DYMCOM project, and the Institute Pascal, University Paris-Saclay for the warm hospitality during the DYMCOM workshop. This work was supported by the Programme National 'Physique et Chimie du Milieu Interstellaire' (PCMI) of CNRS/INSU with INC/INP co-funded by CEA and CNES. JZsM thanks the financial support of the National Research, Development and Innovation Fund of Hungary, under the K 18 funding scheme with project no. K128621.

Data Availability

The data that support the findings of this study are available from the corresponding author upon reasonable request.

References

-
- [1] V. A. Krasnopolsky, *Icarus* **236**, 83 (2014).
 - [2] J. L. Elliot, D. F. Strobel, X. Zhu, J. A. Stansberry, L. H. Wasserman, and O. G. Franz, *Icarus* **143**, 425 (2020).
 - [3] V. A. Krasnopolsky, *Icarus* **335**, 113374 (2020).
 - [4] L. A. Young, F. Braga-Ribas, and R. E. Johnson, in *The Trans-Neptunian solar system*, edited by D. Prialnik, M. A. Barucci, and L. A. Young (Elsevier, The Netherlands, 2020), chap. 6, pp. 127–151.
 - [5] R. A. Armstrong, D. M. Suszcynsky, W. A. Lyons, and T. E. Nelson, *Geophys. Res. Lett.* **27**, 653 (2000).
 - [6] M. Oberkofler and *et al*, *Journal of Nuclear Materials* **438**, S258 (2013).
 - [7] C. Giroud, *et al*, and JET-EFDA contributors, in *Proceedings of the 23rd IAEA Fusion Energy Conference, Daejeon, 11-16 October 2010* (International Atomic Energy Agency, 2010).
 - [8] V. Laporta, R. Celiberto, and J. M. Wadehra, *Plasma Sources Science and Technology* **21**, 055018 (2012), URL <http://stacks.iop.org/0963-0252/21/i=5/a=055018>.
 - [9] V. Laporta, D. A. Little, R. Celiberto, and J. Tennyson, *Plasma Sources Science and Technology* **23**, 065002 (2014), URL <http://stacks.iop.org/0963-0252/23/i=6/a=065002>.
 - [10] M. Kitajima, T. Kishino, T. Okumura, N. Kobayashi, A. Sayama, Y. Mori, K. Hosaka, T. Odagiri, M. Hoshino, and H. Tanaka, *Eur. Phys. J. D* **71**, 139 (2017).
 - [11] V. Guerra, P. A. Sa, and J. Loureiro, *The European Physical Journal - Applied Physics* **28**, 125 (2004).
 - [12] M. Panesi, T. E. Magin, A. Bourdon, A. Bultel, and O. Chazot, *Journal of Thermophysics and Heat Transfer* **25**, 361 (2011).
 - [13] M. Capitelli, G. Colonna, G. D'Ammando, V. Laporta, and A. Laricchiuta, *Chemical Physics* **438**, 31 (2014).
 - [14] K. L. Heritier, R. L. Jaffe, V. Laporta, and M. Panesi, *J. Chem. Phys* **141**, 184302 (2014).
 - [15] M. R. Torr, *J. Geomag. Geoelectr.* **35**, 131 (1983).
 - [16] H. Lammer, W. Stumpfner, G. Molina-Cuberos, S. Bauer, and T. Owen, *Planetary and Space Science* **48**, 529 (2000).
 - [17] Y. L. Yung and J. R. Lyons, *Geophysical Research Letters* **17**, 1717 (1990).
 - [18] J. Annaloro and A. Bultel, *Phys. Plasmas* **21**, 123512 (2020).
 - [19] Y. Plastinin, G. Karabadzha, B. Khmelinin, B. Zemliansky, A. Gorshkov, and G. Zalogin, *Measurements of the UV Radiation Generated by the Soyuz Spacecraft Transport Capsule During Reentry* (????), <https://arc.aiaa.org/doi/pdf/10.2514/6.2007-815>.
 - [20] T. Sakakura, N. Murakami, Y. Takatsuji, M. Morimoto, and T. Haruyama, *Chem. Phys. Chem.* **20**, 1467 (2019).
 - [21] I. A. Morozov, A. S. Mamaev, I. V. Osorgina, L. M. Lemkina, V. P. Korobov, A. Y. Belyaev, S. E. Porozova, and M. G. Sherban, *Material Sci. Eng. C* **62**, 242 (2016).
 - [22] M. K. Sharma and B. K. Saikia, *Indian J. Pure and Appl. Phys.* **46**, 463 (2008).
 - [23] J. D. Holcomb and A. Schucker, *Lasers in Surgery and Medicine* **52**, 23 (2020).
 - [24] E. C. Zipf, *Geophysical Research Letters* **7**, 645 (1980).
 - [25] A. J. Cunningham and R. M. Hobson, *J. Phys. B: Atomic and Molecular Physics* **5**, 2328 (1972).
 - [26] S. K. Mitra, *Phys. Rev.* **90**, 516 (1953).
 - [27] J. Kaplan, *Phys. Rev* **73**, 494 (1948).
 - [28] M. A. Biondi and S. C. Brown, *Phys. Rev* **76**, 1697 (1949).
 - [29] C. Noren, F. B. Yousif, and J. B. A. Mitchell, *J. Chem. Soc., Faraday Transactions 2* **85**, 1697 (1989).
 - [30] J. R. Peterson, A. L. Padellec, H. Danared, G. H. Dunn, M. Larsson, A. Larson, R. Peverall, C. Strömholm, S. Rosén, M. af Ugglas, *et al.*, *J. Chem. Phys* **108**, 1978 (1998).
 - [31] D. A. Little, K. Chakrabarti, J. Z. Mezei, I. F. Schneider, and J. Tennyson, *Phys. Rev. A* **90**, 052705 (2014).
 - [32] S. L. Guberman, *J. Chem. Phys* **137**, 074309 (2012).
 - [33] S. L. Guberman, *J. Chem. Phys* **139**, 124318 (2013).
 - [34] S. L. Guberman, *J. Chem. Phys* **141**, 204307 (2014).

- [35] K. Chakrabarti, D. R. Backodissa-Kiminou, N. Pop, J. Z. Mezei, O. Motapon, F. Lique, O. Dulieu, A. Wolf, and I. F. Schneider, *Phys. Rev. A* **87**, 022702 (2013).
- [36] O. Motapon, N. Pop, F. Argoubi, J. Z. Mezei, M. D. Epee Epee, A. Faure, M. Telmini, J. Tennyson, and I. F. Schneider, *Phys. Rev. A* **90**, 012706 (2014).
- [37] M. D. Epée Epée, J. Z. Mezei, O. Motapon, N. Pop, and I. F. Schneider, *Monthly Notices of the Royal Astronomical Society* **455**, 276 (2016).
- [38] A. Abdoulanziz, F. Colboc, D. A. Little, Y. Moulane, J. Z. Mezei, E. Roueff, J. Tennyson, I. F. Schneider, and V. Laporta, *Monthly Notices of the Royal Astronomical Society* **479**, 2415 (2018).
- [39] J. Z. Mezei, K. Chakrabarti, M. D. Epée Epée, O. Motapon, C. H. Yuen, M. A. Ayouz, N. Douguet, S. F. dos Santos, V. Kokoouline, and I. F. Schneider, *ACS Earth Space Chem.* **3**, 2376 (2019).
- [40] D. O. Kashinski, D. Talbi, A. P. Hickman, O. E. Di Nallo, F. Colboc, K. Chakrabarti, I. F. Schneider, and J. Z. Mezei, *J. Chem. Phys.* **146**, 204109 (2017).
- [41] M. J. Seaton, *Reports on Progress in Physics* **46**, 167 (1983).
- [42] J. Tennyson, *Phys. Rep.* **491**, 29 (2010).
- [43] D. A. Little and J. Tennyson, *J. Phys. B: At. Mol. Opt. Phys.* **46**, 145102 (2013).
- [44] D. A. Little and J. Tennyson, *J. Phys. B: At. Mol. Opt. Phys.* **47**, 105204 (2014).
- [45] H.-J. Werner, P. J. Knowles, G. Knizia, F. R. Manby, and M. Schütz, *WIREs Comput Mol Sci* **2**, 242 (2012).